Biosensors and Bioelectronics 198 (2022) 113807

Contents lists available at ScienceDirect

Biosensors and Bioelectronics

journal homepage: www.elsevier.com/locate/bios

A novel electronic tongue using electropolymerized molecularly imprinted polymers for the simultaneous determination of active pharmaceutical ingredients

Mingyue Wang, Xavier Cetó, Manel del Valle *

Sensors and Biosensors Group, Department of Chemistry, Universitat Autònoma de Barcelona, Edifici Cn, 08193, Bellaterra, Barcelona, Spain

ARTICLE INFO

Keywords:
Molecularly imprinted polymers
Electronic tongues
Electrochemical sensors
Artificial neural networks
Pharmaceutical analysis

ABSTRACT

The combination of chemometrics and electrochemical sensors modified with molecularly imprinted polymers (MIPs) towards the development of MIP-based electronic tongues (ETs) was explored herein. To demonstrate the potential of such an approach, the simultaneous determination of paracetamol, ascorbic acid and uric acid mixtures in pharmaceutical samples was evaluated. To this aim, MIP-based sensors for the different compounds were prepared by in situ electropolymerization of pyrrole in the presence of *p*-toluenesulfonate anion (pTS^-), which acted as functional doping ion of the polypyrrole (PPy) MIP backbone. Morphological characterization of the MIPs was done by scanning electron microscopy (SEM), while functionalization of the electrodes was monitored electrochemically. Under the optimized measuring conditions, the developed sensors showed a good performance, with good linearity at the μM level ($R^2 > 0.992$, limits of detection between 1 and 24 μM) as well as good repeatability (intra- and inter-day RSD values between 3 and 6% over 30 consecutive measurements). Finally, the quantification of the individual substances in different pharmaceutical samples was achieved by an artificial neural networks (ANNs) model, showing satisfactory agreement between expected and obtained values ($R^2 > 0.987$).

1. Introduction

The greatly improved life quality and the extended life expectancy of human being witnessed over the past decades can be partly attributed to the ever-increasing use of pharmaceutical drugs against diseases and the more sophisticated methods for detecting key metabolite biomarkers that allow the diagnosis of pathologies.

Traditionally, drugs are administered on the basis of factors such as patients' weight or age, which works for most of the cases. However, certain drugs have a narrower therapeutic window, which can result in a patient easily being under- or over-dosed. The same happens with people who suffer altered metabolism or certain diseases. From this perspective, in comparison to mono-component drugs, multidrug formulations are less harmful because of the smaller incorporated amounts of each active component. Nevertheless, certain combinations of drugs are also likely to lead to unpredictable systemic levels (Hilberg et al., 2005; Meneghello et al., 2018). Thus, despite the great advantages that may offer, those still have some negative effects, especially in cases of overdosing (Bergh et al., 2021; Root-Bernstein et al., 2020). To overcome such scenarios, therapeutic drug monitoring (TDM) is required, so as to ensure individually-directed proper dosing. Therefore, the accurate and rapid analysis of biomolecules and active pharmaceutical ingredients (APIs) aroused keen interest of researchers, pharmaceutical industry and clinicians.

Despite various analytical methods have already been applied for TDM, including high performance liquid chromatography (HPLC), spectrophotometry and titrimetry, drawbacks like being time-consuming, laborious, or expensive are inevitable. Compared with these conventional methods, the combination of electrochemical methods with molecularly imprinted polymers (MIPs) can be a competitive alternative for the detection of biomolecules owing to their numerous advantages such as rapid response, low-cost and high sensitivity and selectivity (BelBruno, 2019; Gui et al., 2018). MIPs are tailor-made biomimetic materials, sometimes referred to as plastic antibodies, not only possessing the "key and lock" specific recognition mechanism owing to the specific sites produced by template molecules, but also with advantages over natural antibodies in terms of reusability, and higher mechanical and chemical stability in harsh conditions (Chen

* Corresponding author. Sensors and Biosensors Group, Universitat Autònoma de Barcelona, Campus UAB, Edifici Cn, 08193, Bellaterra, Spain.
E-mail addresses: manel.delvalle@uab.cat, manel.delvalle@gmail.com (M. del Valle).

https://doi.org/10.1016/j.bios.2021.113807
Received 5 October 2021; Received in revised form 12 November 2021; Accepted 13 November 2021
Available online 17 November 2021

et al., 2011; Rebelo et al., 2021). Hence, MIP-based electrochemical sensors have been research hotspots for their broad-spectrum applications in environmental monitoring (Rebelo et al., 2021), disease diagnosis (Zaidi, 2018), food or medical safety evaluation (Cao et al., 2019) and so on (Herrera-Chacon et al., 2021; Wackerlig and Lieberzeit, 2015).

Among the different approaches for the synthesis of MIPs, electropolymerization is simple, facile, highly reproducible and facilitates the direct integration of MIPs with voltammetric sensors (Arabi et al., 2021; Herrera-Chacon et al., 2021). In this regard, pyrrole (Py) is a well-known functional monomer used to obtain imprinted structures without the necessity of cross-linkers or initiators (Kumar et al., 2021; Zhang et al., 2018). However, anions must be introduced into the polypyrrole (PPy) backbones to ensure its structural stability. Although perchlorate (ClO_4^-) is the most commonly used, different anions can greatly influence the properties of the resulting polymer and its morphology (Bolat et al., 2019; Carquigny et al., 2008; Raudsepp et al., 2008). It has been reported that *p*-toluenesulfonate (pTS$^-$) doped PPy film holds high electrical conductivity, good mechanical properties, higher flexibility and durability, and a micro-porous structure (Rajesh et al., 2004; Raudsepp et al., 2008; Solanki et al., 2007).

Despite the improved sensitivity and selectivity of MIP-based electrochemical sensors, those can still show some cross-response towards other molecules, especially with chemically analogous structures. Moreover, when attempting the multi-determination of several compounds, the use of multivariate regression methods might demonstrate advantageous. In this direction, electronic tongues (ETs) approach may help to overcome such issues (Cetó et al., 2016; del Valle, 2010; Herrera-Chacon et al., 2021). ETs are based on the combination of an array of (bio)sensors able to provide a wide and complete response of the analyzed species, plus a modelling tool able to interpret and extract meaningful data from the complex readings. However, even with the large number of publications reporting the development of MIP-based electrochemical sensors and the great benefits that could be derived from the combination of MIPs with ET approach, few publications exploiting this approach can be found (Herrera-Chacon et al., 2018; Huynh and Kutner, 2015).

In order to demonstrate the potential of MIP-based ETs for TDM, the quantitative analysis of paracetamol (PA), ascorbic acid (AA) and uric acid (AA) mixtures is investigated herein as a proof-of-concept of what can be achieved. Moreover, having as ultimate goal, to provide a generic protocol for the development of MIP-based ETs towards almost any other analyte.

In this context, overdose of PA, which is widely used as an analgesic and antipyretic drug, could lead to fatal hepato- and nephro-toxic effects (Vale and Proudfoot, 1995). Precisely, its wide availability in conjunction with its relatively high toxicity lead to PA being one of the most common causes of poisoning worldwide (Prince et al., 2000). Similarly, AA is a valuable vitamin that is extensively employed in combination with other medicines (such as PA) in the treatment of the common cold (Naidu, 2003). It has been proven that the deficiency of AA is closely related to terrible scurvy, the disturbance in the collagen metabolism and the reduction of women's fertility (Brambilla et al., 2018; Dosedel et al., 2021; Grewal et al., 2019). On the contrary, AA abuse can cause deep vein thrombosis (Bergh et al., 2021). Moreover, some studies have suggested that AA intake is related to UA concentration in body fluids (Huang et al., 2005; Juraschek et al., 2011); the latter being associated with various diseases, such as gout, hyperuricemia or Lesch–Nyhan syndrome, arthritis, diabetes, high cholesterol, renal, neurological, cardiovascular and kidney diseases (Sieminska et al., 2020).

Based on the aforementioned, herein we report on the preparation of three PPy MIP-based sensors for PA, AA and UA in the presence of pTS$^-$ anion through a generic, facile and simple electropolymerization method, and their subsequent integration into a sensor array to construct a voltammetric ET for the simultaneous determination of those three analytes in pharmaceutical samples. The voltammetric responses of the developed MIP-based sensors were firstly characterized to assess the performance of the built sensors. Next, the registered voltammograms were analyzed by chemometric tools to achieve the simultaneous quantification of the ternary mixtures. Benefiting from the complementary advantages of MIPs structure and ETs approach, the MIP-based sensor array exhibited superb sensitivity, selectivity and a wide detection range in the simultaneous determination of PA, AA and UA. Furthermore, the novel ET sensor was successfully applied in the analysis of real pharmaceutical samples.

2. Experimental section

2.1. Reagents and instruments

All the reagents were analytical reagent grade and used in the experiments without any further purification process. Solutions were prepared using deionized water from a Milli-Q System (Millipore, Billerica, MA, USA). Pyrrole (Py), *p*-toluenesulfonic acid (pTS$^-$) sodium salt, potassium chloride, potassium hydrogenphosphate, potassium dihydrogenphosphate, paracetamol (PA), ascorbic acid (AA) and uric acid (UA) were purchased from Sigma-Aldrich (St. Louis, MO, USA). Phosphate buffered saline (PBS 50 mM, pH 7.0) used in this work contained 100 mM potassium chloride. Graphite powder (particle size <50 μm) was bought from BDH Laboratory Supplies (Poole, UK) and epoxy resin kit was supplied by Resineco green composites (Barcelona, Spain).

Scanning electron microscopy (SEM) was observed by EVO MA10 (Zeiss, Oberkochen, Germany) operated at 30 kV.

2.2. Preparation of the pTS$^-$/PPy MIPs and NIP sensors

Hand-made graphite-epoxy composite electrodes (GEC, geometric area of 28.3 mm^2) acted as platforms for the electropolymerization of pTS$^-$/PPy MIPs and non-imprinted polymer (NIP). The construction procedures for GEC are based on previous reports from the group (Alegret et al., 1996). Firstly, the epoxy resin was mixed with its corresponding weight of hardener and graphite powder until completely homogenized. Then, the mixture was loaded into the cavity of a PVC tube, in which a copper disk soldered to a connector had been previously introduced, and dried in the oven at 40 °C for 48h. Finally, the dried GECs are polished with sandpapers of decreasing grain size until a smooth surface was obtained.

For the electropolymerization of pTS$^-$/PPy MIPs onto the GEC electrodes, 20 mL of an aqueous solution containing 0.05 M pyrrole monomer, 0.1 M pTS$^-$ and 0.02M of the template molecule (either PA, AA or UA) were purged with nitrogen for 10 min before cycling the potential from −0.6 V to +0.8 V *vs.* Ag/AgCl at a scan rate of 100 mV s^{-1}. In this manner, replacing the template solution, the different pTS$^-$/PPy MIPs could be obtained. For PA and AA, those were dissolved in Milli-Q water directly. But in the case of UA, due to its lower solubility, UA was firstly dissolved in a NaOH solution (20 mL, pH 10.0) by stirring and sonicating, and then pyrrole and pTS$^-$ were added into the filtered UA solution. Next, in order to extract the template molecules from the PPy film, the electrodes were dipped into PBS and cycled 35 times at a scan rate of 50 mV s^{-1} in the range of −0.6 V to +1.0 V *vs.* Ag/AgCl. Finally, the electrodes were rinsed and kept dry at 4 °C in the fridge when not in use.

For control purposes, the pTS$^-$/PPy NIP modified GEC was prepared following the same procedure as above-mentioned, but without the addition of the template molecules into the polymerization solution. The lack of the template molecule during the polymerization leads to the formation of a polymer with non-specific and non-homogeneous sites, what should clearly demote its selectivity towards the target analyte. Thus, by benchmarking the performance of the MIP against the NIP, it is possible to demonstrate and evaluate the imprinting effect, as it provides a measurement of the specific interactions in the generated MIP sites to the unspecific interactions between the analyte and polymeric material.

2.3. Electrochemical measurements

Electrochemical measurements were all carried out at room temperature, in a multichannel configuration using an Autolab PGSTAT30 (Ecochemie, Netherlands) controlled by GPES Multichannel and FRA software packages. A standard three-electrode cell composed of an Ag/AgCl (3 M KCl) reference electrode, a Pt wire as counter electrode and the modified GECs with pTS$^-$/PPy MIPs and NIP as working electrodes. Electrochemical characterizations of bare and modified GECs were performed by cyclic voltammetry (CV) and electrochemical impedance spectroscopy (EIS) in a 5 mM $K_3[Fe(CN)_6]/K_4[Fe(CN_6)]$ solution in PBS. CV measurements were conducted in the potential range from −0.2 V to +0.7 V at a scan rate of 50 mV s^{-1}. Impedance spectra were recorded in the frequency range between 50 kHz and 50 mHz with a fixed AC amplitude of 10 mV and an applied potential of +0.23 V. For the analysis of the impedance spectra, data was fitted to the Randles equivalent circuit (inset of Fig. 1f), composed of the solution resistance (R_s), the charge transfer resistance between the solution and the electrode surface (R_{ct}), the Warburg impedance (Z_w, related to the diffusion of the electroactive species from the solution towards the electrode surface), and the double-layer capacitance (C_{dl}).

For the analysis of APIs, differential pulse voltammetry (DPV) was the chosen technique. The potential was scanned from −0.4 V to +0.8 V with a step potential of 5 mV and a pulse amplitude of 50 mV without stirring. Before each measurement, the electrodes were immersed for 180 s in the solution to be analyzed under stirring to allow for the enrichment of the analytes in the MIP sites. After each measurement, the electrodes were electrochemically cleaned in PBS by applying a fix potential of +0.8 V for 180 s.

2.4. Samples under study

On the one hand, stock solutions of each of the different APIs were prepared in PBS. From those, intermediate working solutions at different concentrations were prepared by appropriate dilution in PBS, and used to characterize the analytical response of each of the developed MIP-based sensors in terms of linearity, sensitivity, limit of detection (LOD), etc.

On the other hand, for the simultaneous determination of APIs, a set of 38 samples divided into two subsets were prepared by appropriate dilution and mixing of the stock solutions. The first subset used to establish the response model (training subset), was based on a 3^3 tilted factorial design, as shown in Fig. S1. The concentrations for each of the compounds were in the range 0–50 μM for PA, 0–1000 μM for AA and

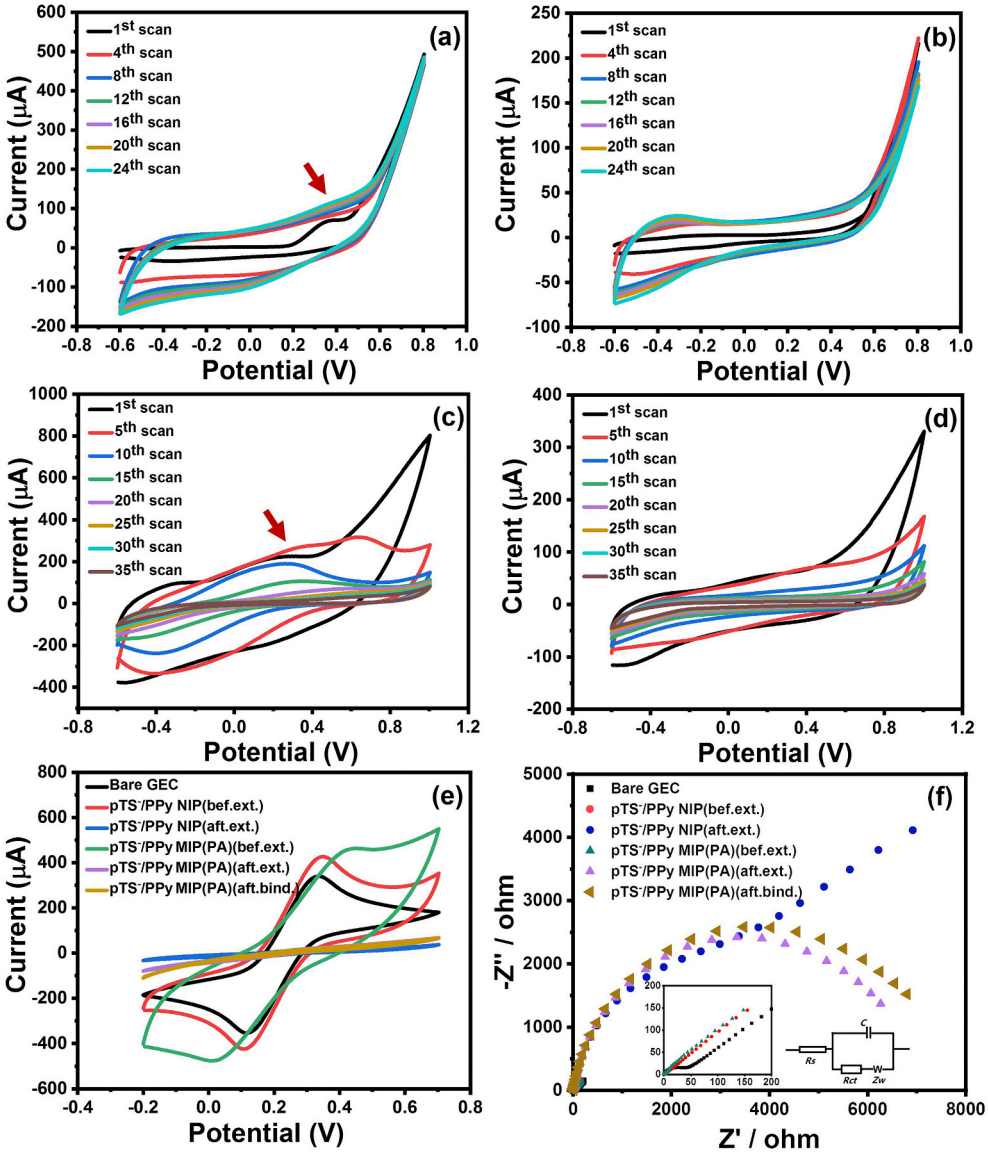

Fig. 1. Cyclic voltammograms taken during the electropolymerization of pTS$^-$/PPy onto a GEC (a) with paracetamol (MIP(PA)) and (b) without template molecule (NIP). Cyclic voltammograms taken during the template extraction of (c) pTS$^-$/PPy MIP(PA) and (d) pTS$^-$/PPy NIP. (e) Voltammetric and (f) impedimetric responses towards a 5 mM $[Fe(CN)_6]^{3-/4-}$ solution in PBS after each modification step and rebinding experiments: (black) bare electrode, (red and green) after Py electropolymerization, (blue and purple) after extraction of the template, (green and brown) after rebinding of the template. (For interpretation of the references to colour in this figure legend, the reader is referred to the Web version of this article.)

50–500 μM for UA. Next, in order to assess the performance of the built model, a set of 11 samples (testing subset) randomly distributed along the experimental domain defined by the factorial design was also prepared and measured under the same conditions.

Lastly, in order to demonstrate the applicability of the developed ET in real-world scenario, the analysis of commercial tablets bought from local drugstores was attempted. To this aim, tablets were dissolved in PBS so that the expected concentrations fall within the experimental domain of the built model, without requiring further pre-treatment. Furthermore, some of them were also spiked with UA to evaluate its recovery values as well. Concretely, the three following pharmaceutical preparations were evaluated: *Efferaldol* (330 mg paracetamol and 200 mg ascorbic acid (vitamin C); Bristol Myers Squibb, S.A., Madrid), *Multicentrum* (800 μg vitamin A, 15 mg vitamin E, 100 mg vitamin C, 30 μg vitamin K, 1.4 mg thiamine (vitamin B1), 1.75 mg riboflavin (vitamin B2), 2 mg vitamin B6, 2.5 μg vitamin B12, 5 μg vitamin D, 62.5 μg biotin (vitamin B7), folic acid (vitamin B9), 20 mg niacin (vitamin B3), 7.5 mg pantothenic acid (vitamin B5), 162 mg calcium, 125 mg phosphorous, 100 mg magnesium, 5 mg iron, 100 μg iodine, 500 μg copper, 2 mg manganese, 40 μg chromium, 50 μg molybdenum, 30 μg selenium and 5 mg zinc; GlaxoSmithKline España, Madrid) and *Redoxon* (1000 mg vitamin C, 10 mg zinc, 10 μg vitamin D; Bayer Hispania, S.L., Sant Joan Despí).

2.5. Data analysis

Processing of the data was done in Matlab 7.1 (MathWorks, Natick, MA, USA) with the aid of its Neural Network toolbox, while final representation and analysis were done in Origin 2019 (OriginLab Corporation, Northampton, MA, USA). The potential of the ET to discriminate between the different APIs was assessed by means of principal component analysis (PCA), whereas artificial neural networks (ANNs) were chosen as the modelling tool for the quantification of their mixtures. To this end, recorded voltammograms were first compressed by means of discrete cosine transform (DCT) (Cetó and Pérez, 2020), and the obtained coefficients were then submitted to PCA or ANNs.

Briefly, the use of DCT was motivated to reduce the dimensionality and complexity of the voltammetric signals, which allows to gain advantages in the modelling stage such as a reduction in training time, to avoid redundancy in input data and to obtain a model with better generalization ability (Cetó et al., 2013a,b). PCA allows to evaluate samples (dis)similarities and assess initial patterns in the data, whilst ANNs represent a high-performance modelling tool able to achieve the simultaneous multi-determination of the different compounds in mixtures.

3. Results and discussion

As already introduced, the aim of this work is to develop a voltammetric ET consisting of an array of MIP-based sensors targeting a mixture of oxidizable APIs. In this direction, herein we propose a facile and generic strategy for the synthesis of MIPs based on the electropolymerization of Py, an approach that can be easily adapted to different target analytes (the templates). Moreover, another main asset of this approach is that it's a one-step electrochemical-synthesis, which makes the integration of the MIP onto the electrode straightforward, while allowing to control the thickness of the MIP by changing the total charge flown at the electrode, the polymerization media or the electrolyte nature.

Next, the developed sensors are combined into an array, and the registered responses are analyzed by means of different chemometric methods that allow the discrimination or quantification of the substances in the samples. The general procedure for the synthesis and usage of *p*TS$^-$/PPy MIPs with different template molecules is illustrated in Scheme 1.

Such an approach seeks to combine the advantages of MIPs to address the lack of selectivity of sensors used in ETs, with the modelling capabilities of ETs to address possible interferences or matrix effects from MIPs (Herrera-Chacón et al., 2021). The idea is similar to bioETs, but with the advantage of MIPs being cheaper, more stable, more resistant to harsh conditions and tailor-made, offering a suitable receptor to almost any analyte of interest.

3.1. Synthesis and morphological characterization

CV was used for the electropolymerization of Py monomer in the presence of the template molecules (PA, AA or UA) and *p*TS$^-$ as supporting electrolyte and doping counter ion to maintain the electroneutrality of the synthetized polymer. Such procedure includes both the synthesis and immobilization of the MIP onto the electrode in a single step (Özcan and Şahin, 2007). Production of specific MIP sites is favored by hydrogen bonding interactions between the N–H groups of PPy and electron lone pairs of the template molecules. Moreover, compared with small-sized inorganic anions such as ClO_4^-, medium-sized organic ones such as *p*TS$^-$, play an important role in improving the performance of PPy MIPs films. Firstly, with the benzene

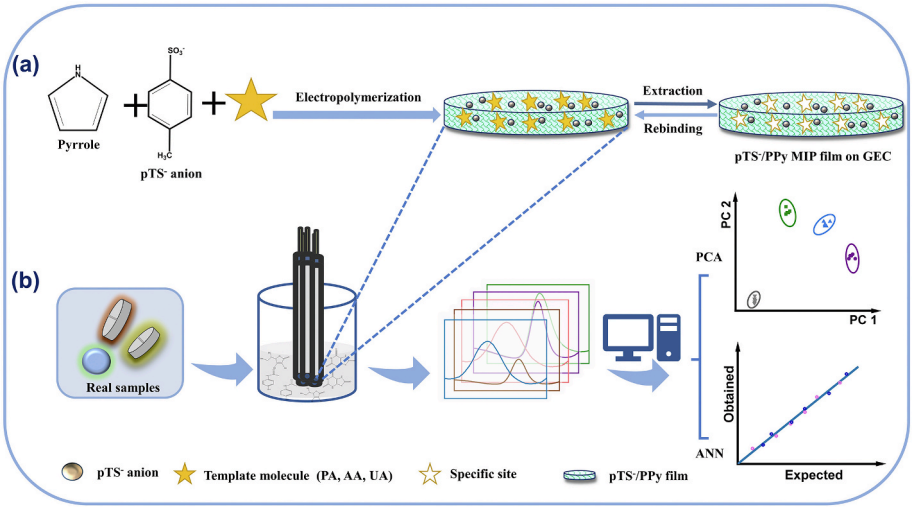

Scheme 1. (a) Preparation of the different *p*TS$^-$/PPy MIPs by electropolymerization of Py in the presence of the template molecules and (b) incorporation of the fabricated MIP-based sensors into the ET sensor array and its application to the analysis of APIs in pharmaceutical samples.

ring, it helps enhancing its binding ability because of the π-π interactions between pTS$^-$ and the analytes. Secondly, PPy films deposited in the presence of such aromatic anions exhibit an anisotropic molecular organization, resulting in higher conductivity and crystallinity (Raudsepp et al., 2008). What's more, as a sulfonate surfactant, pTS$^-$ provides additional benefits by generating higher degree of electrostatic cross-linking and PPy films with a much more microporous structure, which favors a larger sensing surface and higher mass transfer coefficient (Solanki et al., 2007; Suematsu et al., 2000).

The use of amperometric methods allows the control of the polymeric films' thickness by tuning the charge (Coulombs), but even more, CV allows to monitor the entrapment of the template molecules during its growth. As shown in Fig. 1a and b, the capacitive currents increase during the process of electropolymerization with the increase of the number of cycles as a result of the growing thickness of pTS$^-$/PPy film. There are remarkable differences between Fig. 1a and b, where the oxidation peak potential shifts to higher potentials in the presence of PA, suggesting that it is being entrapped into the polymeric chains (Özcan and Şahin, 2007).

Upon synthesis of the MIP, the next step was the removal of the template molecules, which was also done by CV, triggering the recognition at the MIP specific sites. Correspondingly, it can be seen from Fig. 1c that as the number of cycle increases, the oxidation peak of PA disappears gradually, demonstrating that PA molecules are being released. Similarly, electropolymerization and extraction of pTS$^-$/PPy MIP(AA) and pTS$^-$/PPy MIP(UA) are shown in Fig. S2. Due to the different nature and electrochemical behavior of the different template molecules, different voltammetric profiles are obtained during the electropolymerization, but following the same trend overall.

Undoubtedly, the thickness of the modified film plays a crucial role in the performance of the MIP-based sensor, which can be controlled by changing the number of cycles during the electropolymerization. Therefore, the thickness of the film was optimized by changing the number of scans from 8 to 40 cycles (Fig. S3). As can be seen, a low number of cycles leads to higher responses both for the MIP and the NIP as the films are too thin. Oppositely, when this is too high, the MIP behaves similarly as the NIP a fact that can be attributed to the difficulty of the molecules to diffuse through the thicker film, and the difficulty of being oxidized when being too far from the electrode surface due to the low conductivity of the film. Thus, for the selection of the optimal number of cycles, the ratio between the MIP and NIP responses was taken as the selection criteria, selecting 24 cycles as the optimum.

Next, the morphology of the modified electrodes was observed by SEM (Fig. 2). Low magnification images show a homogenous and uniform distribution of pTS$^-$/PPy MIPs and NIP films over the surface of the GEC. From their comparison, it is conspicuous that pTS$^-$/PPy MIPs are rougher than pTS$^-$/PPy NIP, which provides a larger active area for charge and mass transportation. Moreover, to further characterize the synthesized material and confirm the adhesion of the film, elemental composition analysis of the cross-section area for pTS$^-$/PPy MIP(PA) and NIP were measured by energy-dispersive X-ray spectrometry (EDX). Concretely, the analysis of nitrogen, oxygen and sulfur were targeted to confirm the expected composition of the material. A clear change can be observed for nitrogen and oxygen, which confirms the extent of the surface modification of both MIP and NIP as N can be attributed to PPy while sulfur to the doping pTS$^-$ anions.

3.2. Electrochemical characterization

Apart from the morphological characterization, each of the different modification stages was confirmed electrochemically by CV and EIS measurements using $[Fe(CN)_6]^{3-/4-}$ as the redox probe (Fig. 1e and f). Initially, we can see how the bare GEC displays the typical reversible peaks of $[Fe(CN)_6]^{3-/4-}$, while the overall current increases slightly due to the higher capacitive component after the electropolymerization, confirming the attachment of PPy onto the electrode surface. The worse electrochemical behavior of the pTS$^-$/PPy MIP was attributed to the presence of the template affecting the conductivity of PPy. Similarly, analyzing the EIS spectra, it can be seen how initially the charge transfer resistance (R_{ct}) is rather small, but still observing the typical semicircle shape, while after the electropolymerization, the R_{ct} decreased significantly as could be expected from the voltammetric measurement. The next step was the extraction of the template, which should release the sites so that the redox probe obtains easier access to the electrode surface. However, the PPy film was over-oxidized during this step, which resulted in a decrease of its conductivity. This is why there is such a large increase in the R_{ct} and, accordingly, a drastic decrease in the voltammogram current if comparing to the one before the removal of the

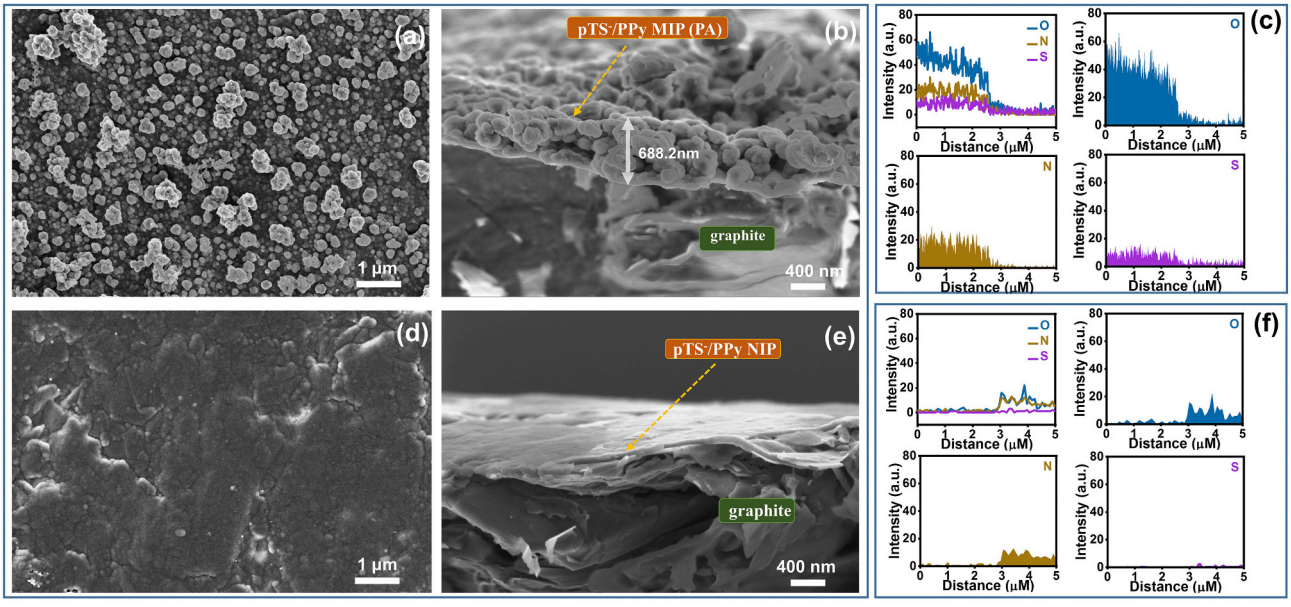

Fig. 2. (a) Top and (b) cross-section SEM images of pTS$^-$/PPy MIP(PA). (d) Top and (e) cross-section SEM images of pTS$^-$/PPy NIP. EDX pattern of (c) pTS$^-$/PPy MIP (PA) and (f) pTS$^-$/PPy NIP; (blue) oxygen, (brown) nitrogen and (purple) sulfur. (For interpretation of the references to colour in this figure legend, the reader is referred to the Web version of this article.)

template. Finally, after the incubation with the template, which is expected to block the diffusion of $[Fe(CN)_6]^{3-/4-}$, a decrease of the voltammetric current and an increase of the R_{ct} upon rebinding of the template molecules with the specific MIP sites was observed. From the voltammetric data, it may hardly be seen how the diffusion of the redox probe was blocked to some extent, but it is much clearer from the Nyquist plot due to the higher sensitivity of the impedimetric measurements. Overall, CV and EIS measurements are in agreement with each other, both confirming the functionalization of the electrode.

3.3. Voltammetric characterization

3.3.1. Calibration curves

The next step before proceeding with the ET approach was the characterization of the electrochemical responses of each sensor towards each considered compound to assess their linear range and sensitivity, as well as confirming that the sensors show certain cross-response and that their responses are stable over time, as otherwise those are not suitable to be used in ETs.

To this aim, calibration curves were built for each of the APIs by DPV due to its higher sensitivity in comparison to CV. However, before proceeding with the electrochemical characterization, the incubation time had to be optimized, taking a compromise between the maximum signal and shorter analysis time (Fig. S4). As could be expected, there is a logarithmic increase of the signal with the incubation time, reaching almost saturation after incubating in the analytes' solution for 180s. Consequently, 180s was taken as the suitable incubation time for further experiments.

The voltammetric responses of the three *p*TS$^-$/PPy MIPs towards increasing concentrations of their respective template molecules are shown in Fig. 3a–c, with current peaks increasing as the concentration increases. From those, the peak heights were calculated and the calibration curves were built (Fig. 3d–f), evidencing a linear trend with high correlation coefficients. Furthermore, not only the response of each MIP was evaluated towards its template, but also the cross-responses towards the other analytes were evaluated (Figs. S5, S6 and S7 as well as Table 1). From the comparison of the calibration curves of the three different *p*TS$^-$/PPy MIPs and the NIP against PA and AA, it can be clearly seen that both MIP-based sensors show higher sensitivity towards their own template molecule than the other sensors (other MIPs and NIP), which demonstrates the specificity of the developed MIPs, but also that there is still some degree of cross-response. However, the fact that *p*TS$^-$/PPy MIP(UA) doesn't show the highest sensitivity to UA may be attributed to the lower solubility of UA in the electrolyte solution, which ultimately affects the number of specific sites generated in *p*TS$^-$/PPy MIP(UA).

Table 1
Analytical parameters of the different *p*TS$^-$/PPy MIPs and NIP towards the three target analytes in PBS extracted from the DPV measurements (results averaged from three different electrodes; the limit of detection (LOD) was calculated on the basis of typical error of the regression line (S/N = 3)).

Analyte	LOD (μM)	Sensitivity (nA·μM^{-1})	Linear range (μM)	R^2
***p*TS$^-$/PPy MIP(PA)/GEC**				
Paracetamol	1.8	139	0.5–50	0.992
Ascorbic acid	177	0.8	500–2000	0.988
Uric acid	1.9	91	2–50	0.994
***p*TS$^-$/PPy MIP(AA)/GEC**				
Paracetamol	177	57	1–1000	0.999
Ascorbic acid	19	18	5–1000	0.997
Uric acid	17	53	0.5–1000	0.997
***p*TS$^-$/PPy MIP(UA)/GEC**				
Paracetamol	1.3	82	0–50	0.997
Ascorbic acid	320	0.2	100–2500	0.983
Uric acid	24	26	50–500	0.996
***p*TS$^-$/PPy NIP/GEC**				
Paracetamol	1.1	78	0.5–50	0.997
Ascorbic acid	157	0.1	500–2500	0.999
Uric acid	3.1	39	5–100	0.996

3.3.2. Repeatability study

Another important feature when developing a sensor, and especially significant from the perspective of ETs, is the repeatability of the developed devices. In order to assess the repeatability, 30 consecutive measurements for each *p*TS$^-$/PPy MIP-based sensor were conducted in their respective template solutions (PA solution was used for NIP-based sensors). After each measurement, electrodes were cleaned in PBS as described in Section 2.3. Furthermore, a blank was also measured in fresh PBS after cleaning as control to evaluate any possible fouling effect. The day-to-day repeatability was evaluated in the same way, using the same MIPs and NIP electrodes during three consecutive days. From those, the relative standard deviation (expressed as percentage, RSD%) were calculated, with values below 6.5% for all the sensors under the two different scenarios (Table S1), asserting that all MIPs and NIP

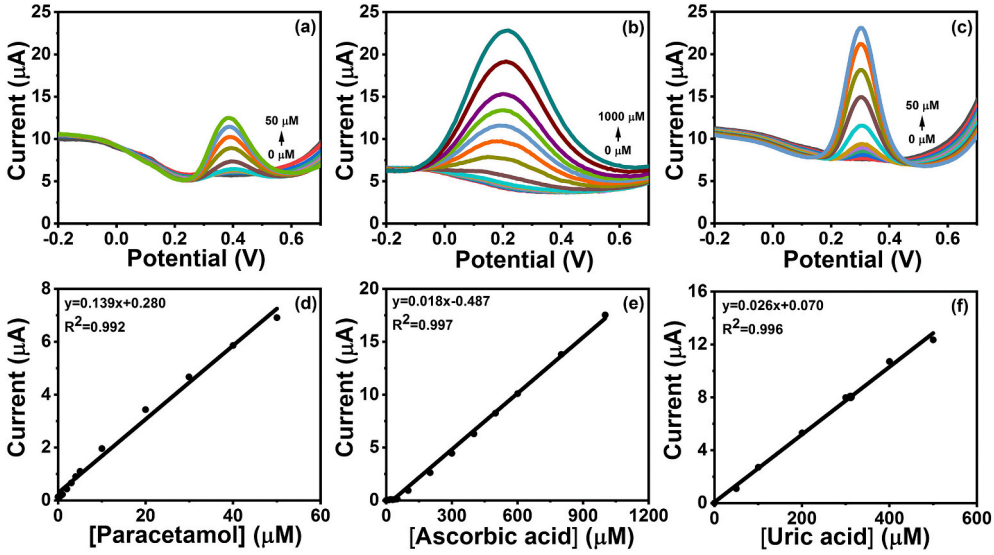

Fig. 3. (Top) DPV responses of the MIP-based sensors towards their respective templates: (a) *p*TS$^-$/PPy MIP(PA) to paracetamol, (b) *p*TS$^-$/PPy MIP(AA) to ascorbic acid and (c) *p*TS$^-$/PPy MIP(PA) to uric acid. (Bottom) Calibration graphs derived from the measured peak heights of *p*TS$^-$/PPy MIP(PA), *p*TS$^-$/PPy MIP(AA), *p*TS$^-$/PPy MIP(UA) and *p*TS$^-$/PPy NIP based sensors for the three analytes: (d) paracetamol, (e) ascorbic acid and (f) uric acid.

sensors render great repeatability.

3.4. MIP-based ET

As already mentioned, the use of chemometric methods could assist in improving the selectivity of MIP-based sensors by shifting the complexity from the chemical to the modelling side (Cetó et al., 2016; del Valle, 2010). To demonstrate such a statement, discrimination of the three considered APIs was first attempted by means of PCA from different stock solutions. This represents a preliminary step to confirm that the MIP-based ET is able to discriminate the different compounds, and therefore has the potential to achieve its simultaneous quantification by developing a proper quantitative model (in this case, by means of ANNs) using an appropriate set of samples.

In both cases, the set of samples were measured by the MIP-based sensor array and the recorded voltammograms were then compressed by means of DCT down to 16 coefficients prior to the qualitative analysis by PCA or quantitative modelling by ANNs. This step, apart from denoising the voltammetric data, assists in reducing the complexity of the input signal, which in turn allows to obtain simpler and more robust models (Cetó et al., 2013a,b).

3.4.1. Qualitative analysis

Under the described conditions in Section 2.3, five replicate samples of 50 μM solutions of each of the APIs were measured employing the developed sensor array (3 MIPs plus the NIP) and then submitted to DCT-PCA.

The main advantage of PCA is allowing to summarize the information contained in large data sets (e.g., the four voltammograms registered with the different sensors for each sample) down to a two- or three-coordinates point in a scores plot, where all the considered samples are also represented. Thus, it provides a better representation of samples (dis)similarities and allows to rapidly detect and assess initial patterns in the data.

The obtained 2D score plot is shown in Fig. 4a, with a cumulative variance of ca. 91.2%, a large value denoting that almost all the variance present in the original data is now summarized with only the first two principal components (PCs). More significantly, we can see how clear clusters are obtained for each of the APIs as well as for the buffer solution, all of them clearly separated with very small confidence intervals

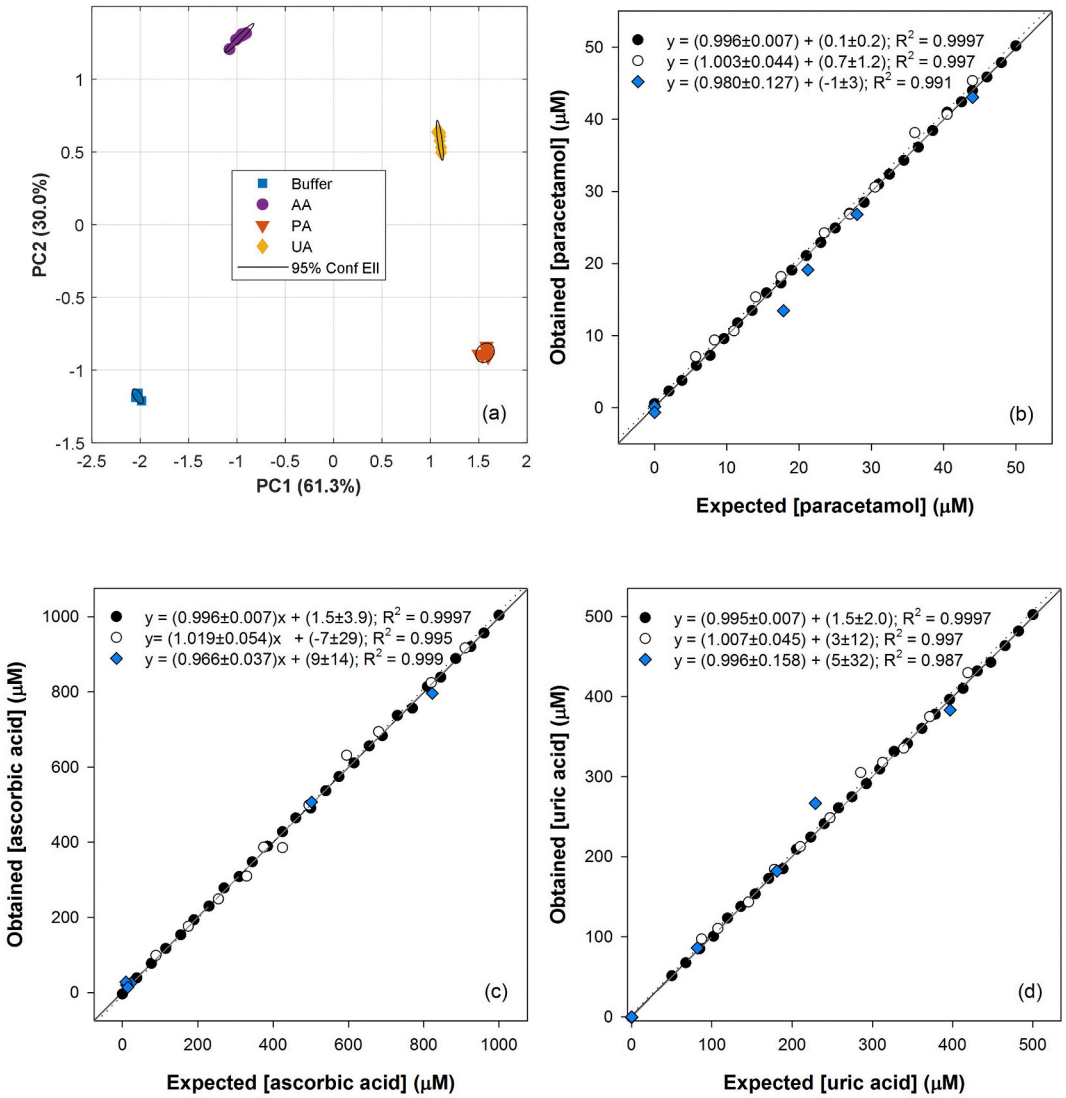

Fig. 4. (a) Score plot of the first two principal components obtained from the DCT-PCA of the voltametric responses of the *p*TS$^-$/PPy MIPs and NIP modified sensors towards: (■) PBS, (▼) paracetamol, (●) ascorbic acid and (♦) uric acid. Ellipses plotted correspond to 95% confidence limits for each of the clusters. (b,c,d) Modeling ability of the optimized DCT-ANNs. Comparison graphs of obtained *vs.* expected concentrations for (b) paracetamol, (d) ascorbic acid and (d) uric acid, for both the training (●, solid line) and testing subsets (○, dotted line). Dashed line corresponds to the ideal comparison line (y = x). Additionally, the results of the analysis of the pharmaceutical samples are also plotted (♦).

for each of the groups. The clustering is so clear that either PC1 or PC2 would be enough to distinguish the different compounds, with the buffer being in one of the extremes of the plot, further from any other cluster.

Moreover, from the comparison of the current PCA plot with the ones reported in previous publications based on arrays of graphite epoxy composites (GECs)(Sarma et al., 2020) or screen-printed electrodes (SPEs)(Ortiz-Aguayo et al., 2019) modified with different electrocatalysts such as Prussian blue or metallic nanoparticles (representing a "conventional" voltammetric ET), we can see how the combination of MIPs and ETs significantly improves the former.

To numerically quantify this improvement, Silhouette clustering metric was considered (Kaufman and Rousseeuw, 1990). Silhouette index provides a measure of how good the clustering is by comparing the intra-cluster distances (cohesion) with respect to the intra-cluster distances (separation). Its value is normalized between −1 and +1, where high values are indicative of good clustering (highly cohesioned groups with good separation between them), and oppositely, low values indicate very poor separation between clusters. The cohesion can be interpreted as a measure of sensors' reproducibility, while separation as a measure of the sensor capability to discriminate the considered compounds.

In our case, the Silhouette index calculated from the PCA score plot was 0.998 (a high value very close to the index maximum), while this was 0.947 and 0.838 for the above-mentioned GEC- and SPE-based ETs. The highest value of the current approach is related to the highest selectivity and specificity of MIPs, while in the case of the GECs, the improved performance arises from a preliminary optimization on the sensors that constituted the ET. Thus, these values confirm the higher performance of the MIP-based ET approach and its potential to succeed in the simultaneous quantification of APIs mixtures.

3.4.2. Quantitative analysis

The set of samples described in section 2.4 were prepared and analyzed under the same conditions as earlier, recording a voltammogram for each of the sensors. As can be seen from Fig. S8, despite each MIP-based sensor responds mainly to its target analyte, there is still some cross-response and peak overlapping for certain samples, hampering the quantification of each API from the univariate regression curves. Nevertheless, as demonstrated with PCA, the use of chemometric methods can greatly assist in improving MIPs' selectivity. Thus, an ANN model was used to achieve the simultaneous determination of the three APIs. The whole set of voltammograms were compressed with DCT and the ANN model was built employing the data of the train subset, using the data of the test subset to assess its performance. This data splitting was done to ensure that the system was not over-fitted, providing a more realistic evaluation of the model performance as test data was not used at all during the modelling stage.

The topology of the neural network was optimized by systematically varying the number of neurons in the hidden layer as well as the transfer functions between the different layers. After the optimization, the selected ANN model had 64 neurons in the input layer (corresponding to the DCT coefficients for each of the sensors), 4 neurons and *purelin* transfer function in the hidden layer, and 3 neurons (one for each of the APIs) and *purelin* transfer function in the output layer.

To visualize the performance of the model, the comparison graphs of obtained *vs*. expected concentrations were built for each of the analytes (Fig. 4b–d), and the equations of the linear regressions as well as their confidence intervals calculated (Table S2). As shown, an excellent agreement is attained with regression lines almost indistinguishable from the theoretical ones, demonstrating the superb specificity derived from the combination of MIPs and chemometrics. This good behavior is also confirmed numerically from the slope, intercept and correlation coefficient values, which are all close to the ideal values (1, 0 and 1, respectively). Additionally, the root mean square error (RMSE) and its normalization (NRMSE) were also calculated to obtain a unique metric of the overall model performance.

To evaluate the improvement derived from the usage of the proposed MIP-based sensor array, the same set of samples were also measured employing a bare GEC electrode, and the data was processed in the same way. After optimization of the ANN topology, a total NRMSE of 0.084 was obtained; a value that is significantly larger than the one of the MIP-based ET, which was 0.020.

Lastly, to benchmark the performance of the MIP-based developed ET, the obtained results were compared to the ones reported in previous works in which the same mixtures were analyzed (Table S2) (Cetó et al., 2013a,b; Gutés et al., 2007; Ortiz-Aguayo et al., 2019; Sarma et al., 2020). Despite it has to be reckoned that some of the differences attained in the final performance originate from the modelling stage itself, that is, depending on the choice of the machine learning algorithms, it can be neglected that the richer and more relevant the raw data is, the better performance will be attained. From the comparison, we can see how the current approach clearly outperforms all the previous reported ETs, therefore, further confirming the benefits derived from the combination of MIPs and ETs.

3.4.3. Real sample analysis

Finally, after generating and validating the performance with the samples of the training and testing subsets, respectively, the developed ET was applied to the analysis of some pharmaceutical preparations. The pharmaceutical samples were prepared as described in Section 2.4 and measured as previous, without performing any sample pre-treatment step. Obtained voltammograms were compressed with DCT and fed to the ANN model which provided the actual amount of API present in the pharmaceutical formulation after multiplying by the proper dilution factor.

In this manner, the analysis of seven different samples prepared from raw and spiked dilutions of the three different pharmaceutical formulations was carried out, and the results are summarized in Fig. 4 and Table S3. As can be observed, a good agreement between obtained and expected values is obtained, again being the values for the slope and intercept close to the ideal ones and within the confidence interval. This is highly relevant as pharmaceutical formulations have a relatively complex matrix with many compounds (excipients, fillers, disintegrants, binders, etc.) or other APIs not considered when building the chemometric model. However, it is evident that those do not affect the performance of the model, as no significant differences are found between the results derived from the stock solutions and the pharmaceutical tablets. This can be attributed not only to the use of ETs, which are known to allow minimizing possible matrix effects, but especially favored by the higher selectivity of the used MIP-based sensors.

4. Conclusions

The potential and advantages derived from the incorporation of MIPs into the ET sensor array have been demonstrated herein through the analysis of APIs mixtures. For the development of the MIP-based ET, a generic facile electropolymerization method of Py in the presence of pTS$^-$ and the target analytes (the templates) has been proposed, which lead to the synthesis of a new kind of pTS$^-$/PPy MIPs. Doping of pTS$^-$ anions into the MIPs structures was confirmed from the SEM-EDX analysis. Apart from the SEM morphological characterization, the modification of the electrode was also confirmed electrochemically after the different steps involved in the synthesis of the MIP as well as its application for sensing.

Upon completing the analytical characterization of the pTS$^-$/PPy MIPs, those were combined into a sensor array, and the developed ET was applied towards the simultaneous accurate determination of PA, AA and UA mixtures. Recorded voltammograms were compressed by means of DCT and an ANN model was built, which showed excellent performance in comparison to previously reported ETs attempting the quantification of the same mixtures.

On the one hand, the obtained results prove the high specificity,

great stability and superb resolution of the developed MIP-based sensors. On the other hand, it also demonstrates that the combination of chemometric methods with MIPs represents a very promising approach as evidenced from both the PCA and ANN models. More importantly, the main advantage of the proposed approach is that MIPs towards other molecules might be generated following the same procedure providing a generic protocol for the development of MIP-based ETs towards other analytes. Overall, the development of MIP-based ETs stands for an extremely promising route for a broad-spectrum of sensing applications in TDM, but also in many other fields.

CRediT authorship contribution statement

Mingyue Wang: Investigation, Methodology, Writing – original draft. **Xavier Cetó:** Conceptualization, Methodology, Software, Writing – original draft. **Manel del Valle:** Conceptualization, Methodology, Writing – review & editing, Funding acquisition. All authors have read and agreed to the published version of the manuscript.

Declaration of competing interest

The authors declare that they have no known competing financial interests or personal relationships that could have appeared to influence the work reported in this paper.

Acknowledgments

The authors acknowledge the support of the Spanish Ministry of Science and Innovation (MCINN) through project PID2019-107102RB-C21. M.d.V. thanks the program ICREA Academia.

Appendix A. Supplementary data

Supplementary data to this article can be found online at https://doi.org/10.1016/j.bios.2021.113807.

References

Alegret, S., Alonso, J., Bartrolí, J., Céspedes, F., Martínez-Fàbregas, E., del Valle, M., 1996. Amperometric biosensors based on bulk-modified epoxy graphite biocomposites. Sens. Mater. 8 (3), 147–154. https://myukk.org/SM2017/article.php?ss=10231.
Arabi, M., Ostovan, A., Li, J., Wang, X., Zhang, Z., Choo, J., Chen, L., 2021. Adv. Mater. 33, 2100543–2100575.
BelBruno, J.J., 2019. Chem. Rev. 119 (1), 94–119.
Bergh, M.S., Oiestad, A.M.L., Baumann, M.H., Bogen, I.L., 2021. Int. J. Drug Policy 90, 103065–103069.
Bolat, G., Yaman, Y.T., Abaci, S., 2019. Sens. Actuators B-Chem. 299, 127000–1270008.
Brambilla, A., Pizza, C., Lasagni, D., Lachina, L., Resti, M., Trapani, S., 2018. Front. Pediatr. 6, 126–129.
Cao, Y., Feng, T., Xu, J., Xue, C., 2019. Biosens. Bioelectron. 141, 111447–111464.
Carquigny, S., Segut, O., Lakard, B., Lallemand, F., Fievet, P., 2008. Synthetic Met. 158 (11), 453–461.
Cetó, X., Céspedes, F., del Valle, M., 2013a. Microchim. Acta 180, 319–330.
Cetó, X., Gutés, A., del Valle, M., 2013b. Acta Manilana 61, 39–49.
Cetó, X., Pérez, S., 2020. Talanta 219, 121253–121260.
Cetó, X., Voelcker, N.H., Prieto-Simón, B., 2016. Biosens. Bioelectron. 79, 608–626.
Chen, L., Xu, S., Li, J., 2011. Chem. Soc. Rev. 40 (5), 2922–2942.
del Valle, M., 2010. Electroanalysis 22, 1539–1555.
Dosedel, M., Jirkovsky, E., Macakova, K., Krcmova, L.K., Javorska, L., Pourova, J., Mercolini, L., Remiao, F., Novakova, L., Mladenka, P., 2021. Nutrients 13 (2), 615–648.
Grewal, A.S., Singh, S., Sharma, N., Rani, L., 2019. Int. J. Pharm. Qual. Assur. 10, 605–612, 04.
Gui, R., Jin, H., Guo, H., Wang, Z., 2018. Biosens. Bioelectron. 100, 56–70.
Gutés, A., Calvo, D., Céspedes, F., del Valle, M., 2007. Microchim. Acta 157, 1–6.
Herrera-Chacon, A., Cetó, X., del Valle, M., 2021. Anal. Bioanal. Chem. 413, 6117–6140.
Herrera-Chacon, A., González-Calabuig, A., Campos, I., del Valle, M., 2018. Sens. Actuators B-Chem. 258, 665–671.
Hillberg, A.L., Brain, K.R., Allender, C.J., 2005. Adv. Drug Deliver. Rev. 57 (12), 1875–1889.
Huang, H.Y., Appel, L.J., Choi, M.J., Gelber, A.C., Charleston, J., Norkus, E.P., Miller 3rd, E.R., 2005. Arthritis Rheum. 52 (6), 1843–18477.
Huynh, T.P., Kutner, W., 2015. Biosens. Bioelectron. 74, 856–864.
Juraschek, S.P., Miller 3rd, E.R., Gelber, A.C., 2011. Arthritis Care Res. 63 (9), 1295–1306.
Kaufman, L., Rousseeuw, P.J., 1990. Finding Groups in Data: an Introduction to Cluster Analysis. John Wiley & Sons, Inc, NJ.
Kumar, D.R., Dhakal, G., Nguyen, V.Q., Shim, J.J., 2021. Anal. Chim. Acta 1141, 71–82.
Meneghello, A., Tartaggia, S., Alvau, D.M., Polo, F., Toffoli, G., 2018. Curr. Med. Chem. 25 (34), 4354–4377.
Naidu, A.K., 2003. Nutr. J. 2, 1–10.
Ortiz-Aguayo, D., Bonet-San-Emeterio, M., del Valle, M., 2019. Sensors 19 (15), 3286–3298.
Özcan, L., Şahin, Y., 2007. Sens. Actuators B-Chem. 127 (2), 362–369.
Prince, M.I., Thomas, S.H.L., James, O.F.W., Hudson, M., 2000. The Lancet 355 (9220), 2047–2048.
Rajesh, Takashima, W., Kaneto, K., 2004. React. Funct. Polym. 59 (2), 163–169.
Raudsepp, T., Marandi, M., Tamm, T., Sammelselg, V., Tamm, J., 2008. Electrochim. Acta 53 (11), 3828–3835.
Rebelo, P., Costa-Rama, E., Seguro, I., Pacheco, J.G., Nouws, H.P.A., Cordeiro, M., Delerue-Matos, C., 2021. Biosens. Bioelectron. 172, 112719–112736.
Root-Bernstein, R., Churchill, B., Turke, M., 2020. Int. J. Mol. Sci. 21 (17), 6230–6250.
Sarma, M., Romero, N., Cetó, X., del Valle, M., 2020. Sensors 20 (17), 4798-4712.
Sieminska, E., Sobczak, P., Skibinska, N., Sikora, J., 2020. Med. Hypotheses 142, 109791–109801.
Solanki, P.R., Arya, S.K., Singh, S.P., Pandey, M.K., Malhotra, B.D., 2007. Sens. Actuators B-Chem. 123 (2), 829–839.
Suematsu, S., Oura, Y., Tsujimoto, H., Kanno, H., Naoi, K., 2000. Electrochim. Acta 45, 3813–3821.
Vale, J.A., Proudfoot, A.T., 1995. The Lancet 346, 547–552.
Wackerlig, J., Lieberzeit, P.A., 2015. Sens. Actuators B-Chem. 207, 144–157.
Zaidi, S.A., 2018. Sens. Actuators B-Chem. 265, 488–497.
Zhang, W., Duan, D., Liu, S., Zhang, Y., Leng, L., Li, X., Chen, N., Zhang, Y., 2018. Biosens. Bioelectron. 118, 129–136.